LA-UR-95-2400

JOINT US/RUSSIAN PLASMA FORMATION EXPERIMENTS FOR MAGNETIC COMPRESSION/MAGNETIZED TARGET FUSION (MAGO/MTF)

I. R. Lindemuth, R. E. Reinovsky, R. E. Chrien, J. M. Christian,
C. A. Ekdahl, J. H. Goforth, R. C. Haight, G. Idzorek, N. S. King, R. C. Kirkpatrick,
R. E. Larson, G. L. Morgan, B. W. Olinger, H. Oona, P. T. Sheehey, J. S. Shlachter,
R. C. Smith, L. R. Veeser, B. J. Warthen*, S. M. Younger
Los Alamos National Laboratory, Los Alamos, New Mexico, USA

V. K. Chernyshev, V. N. Mokhov, A. N. Demin, Y. N. Dolin,
S. F. Garanin, V. A. Ivanov, V. P. Korchagin, O. D. Mikhailov, I. V. Mcrozov, S. V. Pak,
E. S. Pavlovskii, N. Y. Seleznev, A. N. Skobelev, G. I. Volkov, V. A. Yakubov
All-Russian Scientific Research Institute of Experimental Physics, Arzamas-16, Russia

July, 1995

Submitted to

The 10th IEEE International Pulsed Power Conference
Albuquerque NM
July 11-13, 1995

---

* E. G. & G./EM, Los Alamos Operations, Los Alamos, NM.

JOINT US/RUSSIAN PLASMA FORMATION EXPERIMENTS FOR MAGNETIC COMPRESSION/MAGNETIZED TARGET FUSION (MAGO/MTF)

I. R. Lindemuth, R. E. Reinovsky, R. E. Chrien, J. M. Christian,
C. A. Ekdahl, J. H. Goforth, R. C. Haight, G. Idzorek, N. S. King, R. C. Kirkpatrick,
R. E. Larson, G. L. Morgan, B. W. Olinger, H. Oona, P. T. Sheehey, J. S. Shlachter,
R. C. Smith, L. R. Veeser, B. J. Warthen*, S. M. Younger
Los Alamos National Laboratory, Los Alamos, New Mexico, USA

V. K. Chernyshev, V. N. Mokhov, A. N. Demin, Y. N. Dolin,
S. F. Garanin, V. A. Ivanov, V. P. Korchagin, O. D. Mikhailov, I. V. Morozov, S. V. Pak,
E. S. Pavlovskii, N. Y. Seleznev, A. N. Skobelev, G. I. Volkov, V. A. Yakubov
All-Russian Scientific Research Institute of Experimental Physics, Arzamas-16, Russia

Magnetic Compression/Magnetized Target Fusion (MAGO/MTF) is an area of fusion research that is intermediate between Magnetic Fusion Energy (MFE) and Inertial Confinement Fusion (ICF) in time and density scales. This concept has been pursued independently in Russia as MAGO (MAGnitnoye Obzhatiye, or magnetic compression) [1-2] and in the US [3-4]. MAGO/MTF uses a pusher-confined, magnetized, preheated plasma fuel within a fusion target. The magnetic field suppresses losses by electron thermal conduction in the fuel during the target implosion heating process. Reduced losses permit adiabatic compression of the fuel to ignition temperatures even at low (e.g., 1 cm/μs) implosion velocities. In MAGO/MTF, the convergence ratio of the pusher in quasi-spherical geometries may potentially be less than 10, depending upon the initial temperature of the fuel and the adiabaticity of the implosion. Previous work relevant to MAGO/MTF includes, but is not limited to, work in imploding liner fusion, impact fusion and electron-beam driven "phi" targets.

MAGO/MTF has not been extensively pursued, in part because of the challenges associated with developing and mating the two elements of an MTF system: (a) a target implosion system (b) a means of preheating and magnetizing the thermonuclear fuel prior to implosion. The advent of 200-MJ-class disk flux compression generators [5,6] make it possible to consider direct magnetic implosion [2] of fusion targets to ignition conditions in an energy-velocity space simply inaccessible by any other laboratory means [7]. Such energy-rich sources appear ideal for MAGO/MTF and, consequently, for a demonstration of fusion ignition, without a major capital investment in driver technology.

In this paper we report the results of experiments exploring a scheme [8-10] for forming a hot, magnetized plasma possibly suited for subsequent implosion in a MAGO/MTF context. The experiment described here used a plasma formation chamber shown in Fig. 1. The outer radius of the plasma volume was 10 cm. The chamber was initially filled with 10 Torr of 50% deuterium, 50% tritium gas seeded with 0.01% neon. The chamber behavior was computationally modeled using two dimensional magnetohydrodynamic techniques [11].

The chamber was powered by an explosively powered high-gain helical flux compression generator. The electrical circuit is shown in Fig. 2. During the early operation of the generator, explosively operated closing switch S2 was open, and a slowly rising pulse of electrical current was delivered to the chamber to magnetize the gas. At a prescribed time, the explosively operated opening switch R rapidly increased its resistance and a rapidly increasing electrical current pulse was delivered to the chamber to drive the discharge.

The measured chamber input current is shown in Fig. 3a. At 347 μs (t_0), 2.7 MA were delivered to the chamber and magnetic probes interior to the chamber probe confirm that all of the initial, slowly rising current was carried in the chamber walls, encircled the gas volume and

---

* E. G. & G./EM, Los Alamos Operations, Los Alamos, NM.

provided an initial, "bias" magnetic field. Upon operation of the opening switch at 347 μs, the current flowing to the input of the chamber increased to 7.5 MA in 2.5 μs with a peak dI/dt of approximately 3 MA/μs. Inductive probe measurements indicated that the rapidly rising resistance of the opening switch created a voltage sufficient to induce electrical breakdown somewhere within the gas in the chamber.

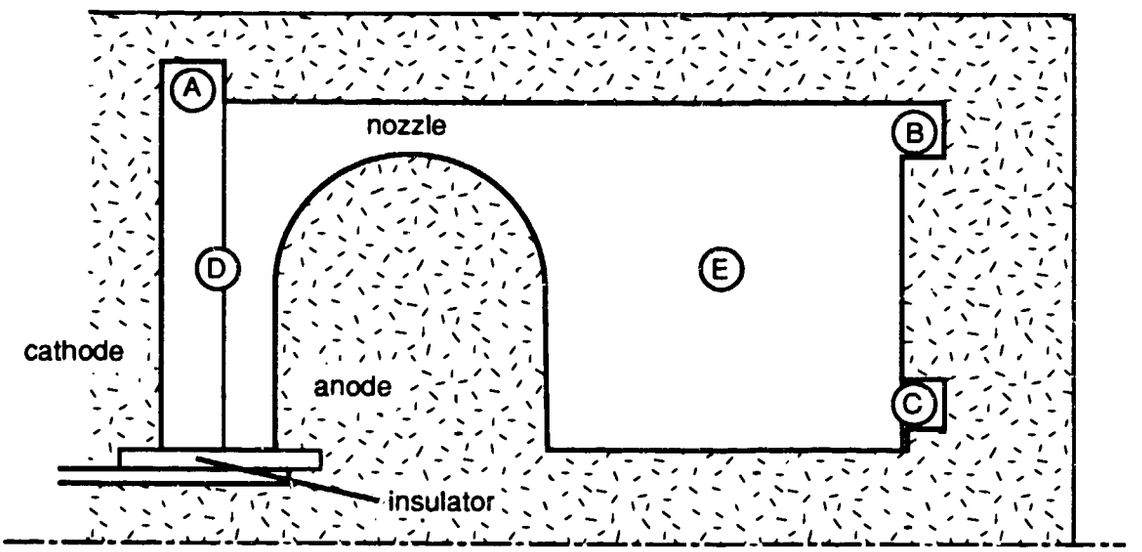

Fig. 1. The plasma formation chamber; points A, B, and C indicate the location of inductive probes; points D and E indicate chordal lines of sight for plasma laser interferometry.

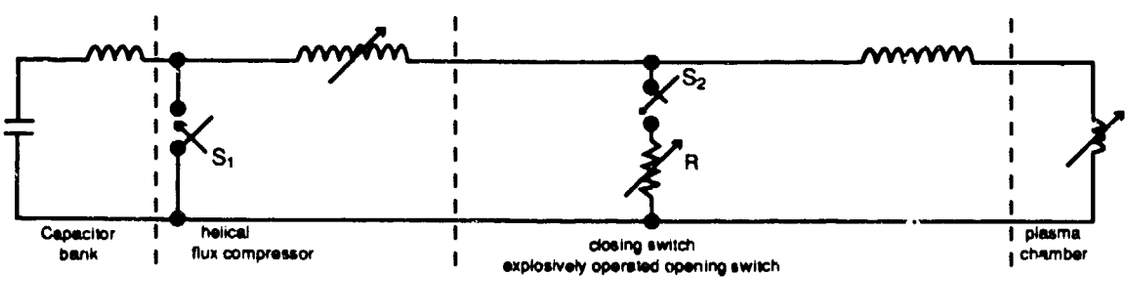

Fig. 2. Idealized electrical circuit diagram; the transformer coupling between the capacitor bank and the helical generator is not shown; also not shown are resistive losses in the circuit.

Figure 3 shows the measured (curve b) and computed (curve c) signals from an inductive probe located at point A of Fig. 1. For approximately 1.3 μs, the signal measured by the probe (curve b) closely followed the chamber input current (curve a). At 1.3 μs, the probe signal (curve b) became almost constant, while the chamber current (curve a) continued to rise, indicating the conduction of current somewhere between the insulator and the probe. According to the computations, this current drove an inverse z-pinch in the left-hand side of the chamber. At 1.5 μs, the probe signal deviated noticeably from the input current, and at about 1.8 μs, a series of oscillations with a peak-to-peak amplitude of approximately 0.75 MA was observed, indicating the arrival of compression waves in the vicinity of the probe and subsequent reflections from the chamber wall and the magnetic piston.

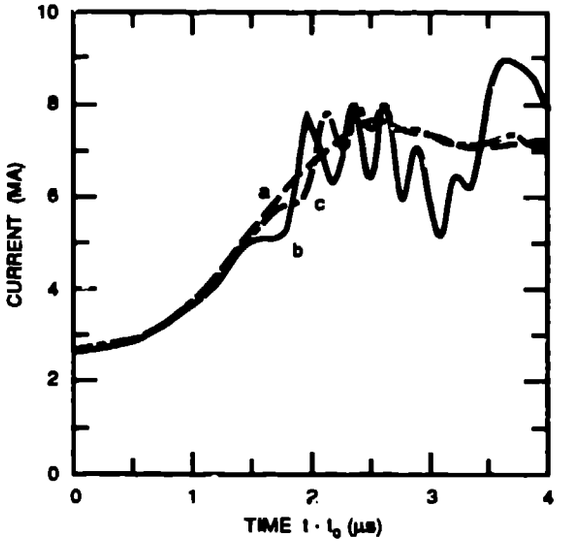

Fig. 3. Inductive probe signals (t_0=347 μs): (a) chamber input current; (b) current measurement at location A of Fig. 1; (c) computation for location A.

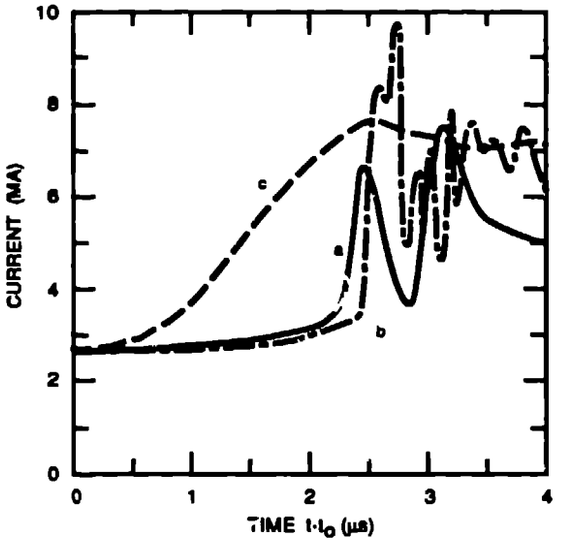

Fig. 4. Inductive probe signals: (a) chamber input current; (b) current measurement at location B of Fig. 1; (c) computation for location B.

Until 2.3 μs, the measured and computed probe signals at location B (Fig. 4, curves b and c, respectively) increased only slightly from the initial 2.7 MA and were significantly less than the chamber input current, indicating most of the rapidly rising input current flowed from the central anode to the outer chamber wall between probes A and B. This approximately radial current drove a shock wave into the right hand side of the chamber. At approximately 2.3 μs, the experimental probe at location B showed the onset of oscillations of approximately 2 MA, indicating the arrival of a current sheath in the vicinity of the probe.

The inductive probe at point C (Fig. 5, curves b and c) showed a similar slow rise for about 2.4 μs, then an approximately monotonic increase at a rate of approximately 2 MA/μs. The slow initial rise in the probes at B and C was due to compression of the initial magnetization flux by the conducting gas piston driven by the current in the nozzle. Even as late as 4 μs, the probe signal at C value did not reach the full input current, indicating current flow from the central electrode to the right hand wall between probes B and C.

Figure 6 shows the results of laser interferometry along chord D in Figure 1 in the left-hand section. Curve a shows an abrupt increase in line-averaged electron density at 1.2 μs, indicating arrival of the radially expanding inverse z-pinch plasma sheath. The density reached a peak value of approximately 2.2 x $10^{17}/cm^3$ and by 2.5 μs decreased to a value 5 x $10^{16}/cm^3$. Because the initial fill density, if fully ionized, is 7 x $10^{17}/cm^3$, the peak value of curve a indicates that the inverse pinch was not fully ionizing. The decrease in density was followed by an increase for about 0.5 μs, at which time the quadrature signals of the interferometer became uninterpretable.

An interferometric measurement along chord E in the right-hand chamber section returned useful data for only about 100 ns after the appearance of plasma in its line-of-sight (Fig. 3, curve c), indicating the time of plasma appearance at 1.7 μs. The computations (curve d) then show a

rapid rise to 1.25 x $10^{18}/cm^3$, a subsequent drop and then oscillatory behavior. The first peak indicates that the gas was fully ionized by the compression wave driven from the nozzle and the subsequent behavior indicates plasma compression towards the axis at smaller radius than the chordal line-of-sight.

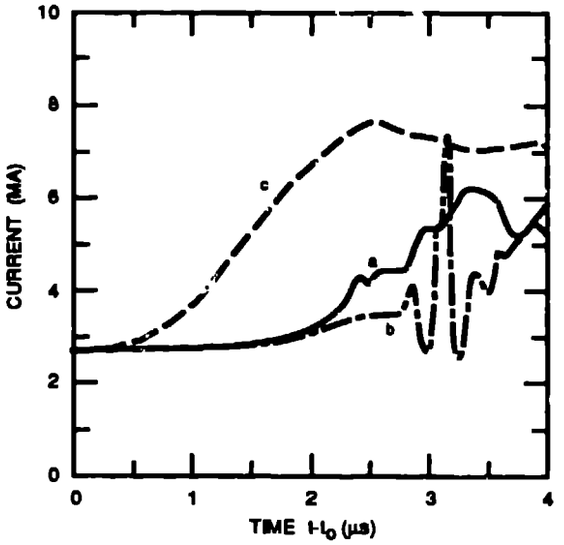

Fig. 5. Inductive probe signals: (a) chamber input current; (b) current measurement at location C of Fig. 1; (c) computation for location C.

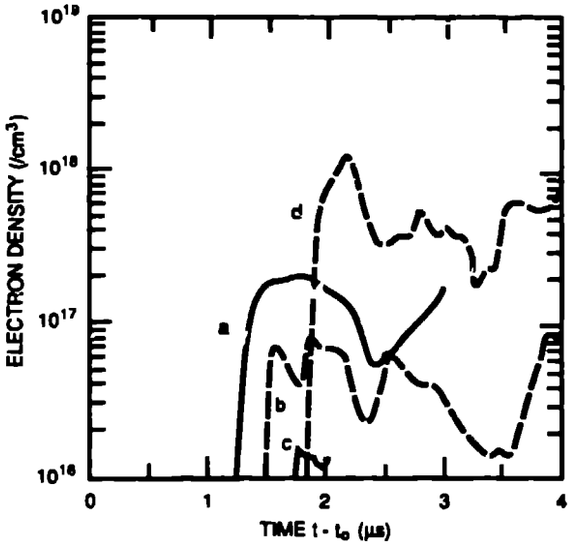

Fig. 6. Chordal line-of-sight interferometric line-averaged electron density: (a) left-hand section of chamber; (b) computation for left-hand section; (c) right-hand section; (d) computation for right-hand section.

Signals from two of four filtered silicon x-ray detectors are shown in Figures 7 (curves a and b). Curve c in Figure 7 is the computed time history of the total hydrogenic continuum radiation above 700 eV--the approximate lower cutoff of the two detectors--for approximately the same line-of-sight viewed by the detectors. The x-ray signals indicate the arrival of hot (T > 100 eV) plasma within the detector line-of-sight. The measured signals persist until at least 7 μs giving reason to be optimistic that such a plasma may be suitable for compression on time scales of 5-10 μs.

Neutron activation and time-of-flight measurements indicated the production of 1 x 10^{13} 14.1 MeV neutrons from the deuterium-tritium fusion reaction. The measured neutron emission rate is shown in Fig. 8, curve a. A peak reaction rate of 3 x 10^{13} neutrons per μs with a FWHM of 300 ns was observed. The peak reaction rate occurred at 3.1 μs. The one-temperature (T_i=T_e) computations reported in this paper also give a neutron peak at approximately the same time with a similar pulse width (Fig. 8, curve b). However, the total yield is approximately two orders of magnitude too low. Two-temperature ideal gas computations (separate T_i, T_e; initially T_i=T_e=2 eV) more closely match the observed yield but do not match the inductive and interferometric measurements because of the high initial electrical conductivity of the entire gas within the chamber.

The computations indicate that the gas that was originally in the left-hand section is compressed by the inverse pinch and accelerated through the nozzle. Upon exiting the nozzle, the fast-moving (20-100 cm/μs) plasma contacts the compressed plasma of the right-hand section

and its kinetic energy is converted to thermal energy. Some plasma (< 5%) reaches temperatures higher than 1 keV and it is from this plasma that the thermonuclear neutrons originate. The two-temperature computations suggest that the ion temperature of the neutron producing plasma became significantly higher than the electron temperature.

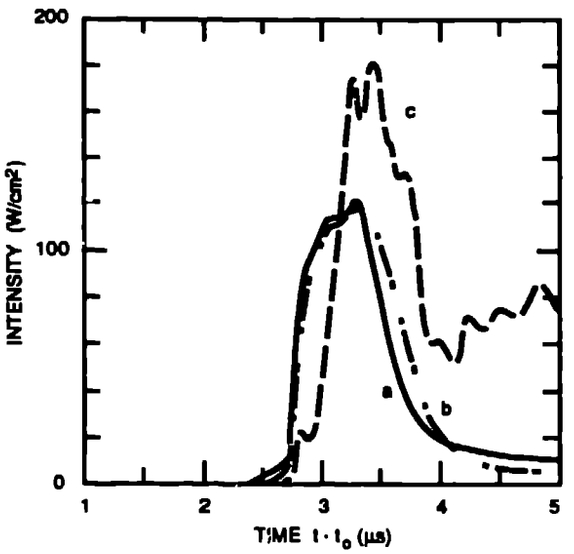

Fig. 7. X-ray signals for right-hand section of chamber, axial view at 6 cm radius: (a), (b) filtered silicon diode detectors; (c) computed hydrogenic continuum above 700 eV.

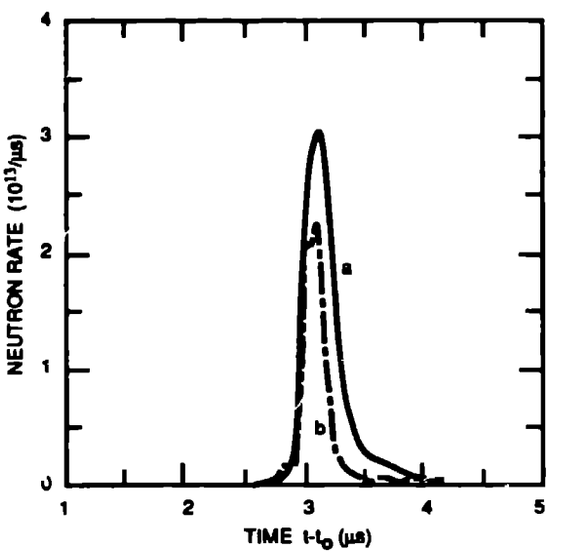

Fig. 8 Neutron emission rate: (a) measured; (b) computed x 50, one-temperature computation (see text).

Like other high-energy-density gas discharge configurations, it would be expected that the plasma would at some time show contamination by wall material (e.g., copper) and that insulator constituents could enter the chamber behind the plasma and possibly mix with the hot plasma during the late times. Spectral measurements performed on the experiment reported here and on earlier experiments have proven inconclusive. An optical multichannel analyzer (OMA) viewing the insulator for a 500 ns window beginning at 1.5 μs showed emitted radiation characteristic of the insulator material as expected, but the qualitative interpretation of the OMA data indicate that the density of insulator material was small. A streak spectrograph viewing the left-hand chamber at chord D of Fig. 1 showed the initiation of the Hβ line at approximately 2.5 μs but did not show indication of any non-hydrogenic species until 4 μs.

For time later than about 4 μs, i.e., after the very complex early-time plasma formation process, the computations show a surprisingly stationary plasma in the right-hand section of the chamber. The plasma can be roughly described as a diffuse, wall-confined z-pinch. The plasma is approximately one-dimensional, with plasma parameters such as density, temperature, and magnetic field varying only with radius. Average computed late-time (10 μs) plasma parameters are n_e=1.6 x 10^{18}/cm^3, ρ=6.7 x 10^{-6} g/cm^3, T=130 eV, B=240 kG, β=0.3, $(\omega\tau)_e$=140. In most diagnostics, the computations show an approximately 200 ns lag when compared to experiment. This lag is eliminated in computations driven by a slightly higher current that is within experimental error. The essential results of the computations are unchanged.

The spherical magnetized target survey model [3] has been used to predict the fusion yield which could potentially be achieved if the plasma formed in the experiment reported here were

subsequently imploded [12]. The computations were based upon the experimental mass (8.9 mg), average computed temperature and magnetic field, and an implosion kinetic energy of 55 MJ. The computations show that unity gain can occur for initial densities above about 10^{-6} g/cm^3 and initial velocities above approximately 0.2 cm/μs. Gains in excess of ten can occur for densities and velocities approximately 2-3 times higher. A gain of 16, and a thermonuclear yield of 1 GJ, is predicted for a density of 6.7 x 10^{-6} g/cm^3, a pusher implosion velocity of 2 cm/μs and a maximum radial convergence of less than 20. The survey computations show that the 290 eV average temperature computed for an earlier, lesser diagnosed experiment can significantly reduce the convergence required and that approximately adiabatic compression can be expected for initial magnetic fields as low as 75 kG.

The survey results coupled with the two-dimensional computations suggest that a plasma suitable for subsequent implosion in a MAGO/MTF context has been produced in the experiment reported here. Further plasma formation experiments are required before the present plasma chamber can be confidently mated with an implosion system. Future experiments will emphasize characterization of the late time plasma behavior and will search for wall and insulator impurities which would degrade the implosion heating process by enhancing the radiation energy losses from the plasma. Although it is quite plausible that the present plasma chamber could be scaled to a smaller size, reducing the implosion energy required, existing high-explosive pulsed power devices [5-7] are sufficient to provide the 65 MJ of energy used in the survey computations.

The experiment reported in this paper is one of several endeavors in the area of pulsed power and ultrahigh magnetic fields conducted as part of scientific collaboration between institutions in the United States and the Russian Federation which have historically had the development of nuclear weapons as their major mission [13]. This collaboration would not have been possible without the support and encouragement of many officials of the governments of Russia and the United States and many administrators and colleagues at the All-Russian Scientific Research Institute of Experimental Physics and the Los Alamos National Laboratory.

REFERENCES

[1] Yu. B. Khariton *et al.*, Uspekhi Fiz. Nauk. **120**, 706 (1976).
[2] V. N. Mokhov *et al.*, Sov. Phys. Dokl. **24**, 557 (1979).
[3] I. R. Lindemuth and R. C. Kirkpatrick, Nuclear Fusion **23**, 263 (1983).
[4] R. C. Kirkpatrick, I. R. Lindemuth, and M. S. Ward, Fusion Technology **27**, 201 (1995).
[6] P. T. Sheehey *et al.*, Physics of Fluids B **4**, 3698 (1992).
[5] V. K. Chernyshev *et al.*, in *Megagauss Fields and Pulsed Power Systems*, edited by V. Titov and G. Shvetsov (Nova Science Publishers, New York, 1990).
[6] A. I. Pavlovskii *et al.*, *ibid.*
[7] R. E. Reinovsky, I. R. Lindemuth, and S. P. Marsh, in *Digest of Technical Papers: Proc. VIII IEEE Pulsed Power Conf.*, edited by R. White and K. Prestwich (Institute of Electrical and Electronics Engineers, New York, 1991).
[8] A. M. Buyko *et al.*, VANT Ser. Metodiki i Programmy Chislennogo Resheniya Zadach Matematicheskoi Fiziki **3**, 30 (1983).
[9] A. M. Buyko *et al.*, in the *Proceedings of the Third Zababakhin Scientific Talks, Kistym, Russia, January, 1992* (to be published).
[10] V. K. Chernyshev, G. I. Volkov *et al.*, in *Megagauss Magnetic Field Generation and Pulsed Power Applications*, edited by M. Cowan and R. B. Spielman (Nova Science Publishers, New York, 1995).
[11] P. T. Sheehey *et al.*, in these proceedings.
[12] I. R. Lindemuth *et al.*, submitted for publication.
[13] I. R. Lindemuth *et al.*, in these proceedings.